Epithelial tissue geometry directs emergence of bioelectric field and pattern of proliferation

Brian B. Silver[a], Abraham E. Wolf[b], Junuk Lee[c], Mei-Fong Pang[a], and Celeste M. Nelson[a,b,*]
[a]Department of Molecular Biology, [b]Department of Chemical & Biological Engineering, and [c]Princeton Neuroscience Institute, Princeton University, Princeton, NJ 08544

ABSTRACT **Patterns of proliferation are templated by both gradients of mechanical stress as well as by gradients in membrane voltage (Vm), which is defined as the electric potential difference between the cytoplasm and the extracellular medium. Either gradient could regulate the emergence of the other, or they could arise independently and synergistically affect proliferation within a tissue. Here, we examined the relationship between endogenous patterns of mechanical stress and the generation of bioelectric gradients in mammary epithelial tissues. We observed that the mechanical stress gradients in the tissues presaged gradients in both proliferation and depolarization, consistent with previous reports correlating depolarization with proliferation. Furthermore, disrupting the Vm gradient blocked the emergence of patterned proliferation. We found that the bioelectric gradient formed downstream of mechanical stresses within the tissues and depended on connexin-43 (Cx43) hemichannels, which opened preferentially in cells located in regions of high mechanical stress. Activation of Cx43 hemichannels was necessary for nuclear localization of Yap/Taz and induction of proliferation. Together, these results suggest that mechanotransduction triggers the formation of bioelectric gradients across a tissue, which are further translated into transcriptional changes that template patterns of growth.**

Monitoring Editor
Valerie Marie Weaver
University of California, San Francisco

Received: Dec 26, 2019
Revised: Jun 1, 2020
Accepted: Jun 2, 2020

INTRODUCTION

Membrane voltage (Vm) is defined as the electric potential difference between the cytoplasm and the extracellular medium (Lobikin *et al.*, 2012; Adams and Levin, 2013). Vm exerts powerful control over tissue-scale growth and the establishment of proliferation gradients (Yang and Brackenbury, 2013; Levin, 2014) during events such as regeneration (Adams *et al.*, 2006, 2007) and tumorigenesis (Chernet *et al.*, 2016). However, the exact role of Vm in patterning is still largely unclear. Many recent studies examining bioelectricity have aimed to determine how Vm gradients emerge across a tissue to form the bioelectric field (Adams *et al.*, 2007; Beane *et al.*, 2011; Pai *et al.*, 2012; Chernet and Levin, 2013; Yang and Brackenbury, 2013). Generation of this gradient has been hypothesized to require symmetry breaking of an initially homogenous state (Pietak and Levin, 2016). However, the signals that regulate Vm to establish the bioelectric field are not fully understood. Controlled manipulation of the bioelectric field across a tissue could be used to regenerate damaged organs or correct carcinogenic phenotypes (Levin, 2010; Tseng and Levin, 2013).

Mechanical forces play an essential role in coordinating the growth of individual cells and multicellular tissues. For example, reducing cytoskeletal tension by constraining cell spreading can be used to modulate differentiation, proliferation, or death (Dike *et al.*, 1999). Tension can also be controlled by geometry at the multicellular level, with increased rates of proliferation occurring in cells located at the convex edges of tissues (Nelson *et al.*, 2005), regions that are under highest mechanical stress. This led us to question how Vm synergizes with mechanical forces to regulate proliferation across cellular and tissue scales. Mechanosensitive ion channels such as Piezo1/2 provide a direct link between mechanical forces and Vm. These channels open in response to stretch or compression in the plasma membrane, which results from mechanical stimuli within the cellular microenvironment including shear stress, fluid

This article was published online ahead of print in MBoC in Press (http://www.molbiolcell.org/cgi/doi/10.1091/mbc.E19-12-0719) on June 10, 2020.

*Address correspondence to: Celeste M. Nelson (celesten@princeton.edu).

Abbreviations used: CaMKII, calmodulin-dependent protein kinase II; CG1, Calcium Green 1; Cx43, connexin-43; Ecad, E-cadherin; FBS, fetal bovine serum; FRAP, fluorescence recovery after photobleaching; PBS, phosphate-buffered saline; PI, propidium iodide; Vm, membrane voltage.

pressure, and substratum stiffness (Wu *et al.*, 2016). Gap junctions form channels comprised of connexin units that allow ions further propagation of ions between neighboring cells (Evans *et al.*, 2006). However, connexin units can exist on their own in the plasma membrane; these structures, known as hemichannels, can also be opened by mechanical forces (Batra *et al.*, 2012) and permit flux of ions across the membrane. Vm can further influence the concentration of physiologically important ions such as Ca^{2+}, which regulates transcription factors that play a pivotal role in controlling whether a cell proliferates or undergoes apoptosis (Berridge *et al.*, 2000). Notably, intracellular Ca^{2+} influences the nuclear translocation of Yap/Taz (Liu *et al.*, 2019), major effectors of the cellular response to mechanical force. Yap/Taz respond to cytoskeletal tension by controlling the expression of genes that determine cell fate, and patterns of Yap/Taz activation presage patterns of growth in vivo (Dupont *et al.*, 2011; Schlegelmilch *et al.*, 2011; Piccolo *et al.*, 2013).

We used epithelial tissues of defined geometry to examine the synergy between mechanical stresses and the Vm gradient, as well as the downstream consequences on cellular behavior. Since depolarization has previously been correlated with proliferation (Adams *et al.*, 2006, 2007; Levin, 2010; Beane *et al.*, 2011; Pai *et al.*, 2012; Chernet and Levin, 2013; Tseng and Levin, 2013; Yang and Brackenbury, 2013; Levin, 2014; Chernet *et al.*, 2016; Levin *et al.*, 2016; Pietak and Levin, 2016), we hypothesized a link among tissue geometry, mechanical stress, and the establishment of bioelectric and proliferation gradients. In these epithelial tissues, we observed the emergence of bioelectric gradients that depend on tissue geometry and that correlate with patterns of mechanical stress. Specifically, cells located at the tissue periphery are more depolarized than cells located in the center of the tissue or at low-tension concave edges. We found that patterned depolarization is required to establish the gradient in proliferation across the tissue. Furthermore, we observed that inhibiting connexin-43 (Cx43) hemichannels abolished the gradient of Vm induced by mechanical stress. We identified Yap/Taz as critical downstream targets of Cx43 hemichannels and Vm signals in the emergence of the proliferation gradient. These data suggest that Vm connects mechanical forces within the microenvironment with transcriptional regulation to drive patterning of proliferation throughout an epithelial tissue.

RESULTS

We used microengineering approaches to create uniform arrays of epithelial tissues of precise geometry (Tan *et al.*, 2004). Mammary epithelial cells formed confluent monolayers that conformed to the geometry of micropatterned islands (Figure 1A), with cell–cell adhesions characteristic of epithelial tissue (Figure 1B). We found that cells located at the periphery of the tissues expressed higher levels of the cell-cycle marker Ki67, as evidenced by immunofluorescence analysis of individual tissues (Figure 1C) and averaging across multiple tissues (Figure 1D). Consistently, cells located at the tissue periphery were also more likely to be actively synthesizing DNA, as revealed by EdU-incorporation assays (Figure 1, E and F). These data are concordant with the results of previous studies that revealed enhanced proliferation of cells located at the edges of epithelial and endothelial tissues (Nelson *et al.*, 2005), where endogenous mechanical stresses are the highest (Figure 1G). This pattern of proliferation was established after 72 h of confluence in mouse mammary tissues, consistent with previous observations of tissues comprised of human mammary epithelial cells (Kim *et al.*, 2009). Sinusoidal tissues that contain both convex and concave regions (Figure 1H) showed elevated proliferation only in the convex regions and decreased proliferation in the concave regions (Figure 1I), suggesting that the emergent pattern of proliferation was not simply due to the presence of an edge in the tissue.

Depolarized Vm has been previously correlated with increased proliferation in tissue-scale patterning events (Yang and Brackenbury, 2013; Levin, 2014, 2016). This led us to ask whether the more proliferative cells located at the tissue periphery were also more depolarized than the less proliferative cells located in the center of the tissue. To measure Vm, we used the anionic voltage-reporter dye $DiBac_4(3)$, which more easily crosses the plasma membrane of more positively charged depolarized cells, leading to an approximately linear increase in fluorescence (Supplemental Figure S1) (Adams and Levin, 2013; Klapperstuck *et al.*, 2013). We found that cells located at the periphery of the tissues were more depolarized than those in the center, as evidenced by the pattern of $DiBac_4(3)$ fluorescence observed in individual tissues (Figure 2A) and in frequency maps of multiple tissues (Figure 2B). Specifically, we found that the average fluorescence at the tissue periphery was 30% higher than that in the center (Figure 2C). Disruption of Vm with gramicidin significantly attenuated this gradient (Figure 2D). We also found a relationship between tissue geometry and the spatial pattern of Vm. Cells in convex (high-stress proliferative) regions of sinusoidal tissues (Gomez *et al.*, 2010) were more depolarized than cells in concave (low-stress nonproliferative) regions (Figure 2, E and F). Similarly, we found that annular tissues exhibited patterns of depolarization along the outer convex edge of the tissue, but not along the inner concave edge (Figure 2, G and H); these patterns of Vm match those of proliferation, which was previously found to be increased at the high-stress outer edge of annuli compared with the low-stress inner edge (Nelson *et al.*, 2005). Cells at the periphery of square tissues were slightly more elongated than cells located in the center of the tissues (Supplemental Figure S2, A and B). However, we found no correlation between $DiBac_4(3)$ fluorescence and either aspect ratio (Supplemental Figure S2C) or circularity (Supplemental Figure S2D), suggesting that the pattern of depolarization was caused by transmission of mechanical stress throughout the tissue rather than by spatial differences in cellular morphology. Treating tissues with the Vm-disrupting drug gramicidin abolished the proliferation gradient, resulting in increased numbers of proliferating cells in the center of the tissues (Figure 2, I and J). Altogether, our data reveal a strong correlation between mammary epithelial tissue geometry and emergent patterns of both proliferation and Vm.

In epithelial tissues, long-range patterns can be established via the transmission of mechanical forces through physical connections between neighboring cells. We previously found that these mechanical stress gradients presage patterns of proliferation within epithelial tissues (Nelson *et al.*, 2005). To determine whether the geometry-induced Vm gradient similarly depends on cell–cell contacts, we created tissues of mammary epithelial cells that do not express the cell adhesion protein E-cadherin (E_{null}) (Figure 3, A and B). EdU analysis revealed a more uniform distribution of proliferation across these tissues (Figure 3, C and D). Consistently, we found that tissues comprised of E_{null} cells also failed to establish a Vm gradient (Figure 3, E–G). In contrast to parental tissues that generated higher mechanical stresses at their periphery, E_{null} tissues showed a uniform pattern of mechanical stress (Figure 3H). These data suggest that the geometry-dependent gradient in Vm requires intact intercellular adhesions between neighboring cells within the epithelial tissue.

To determine whether the Vm gradient is regulated by the intercellular transmission of cytoskeletal tension, we created tissues of mammary epithelial cells that expressed a mutant form of E-cadherin that lacks the β-catenin-binding domain (EΔ) (Figure 4A). Cells in EΔ-expressing tissues formed contacts with their neighbors but

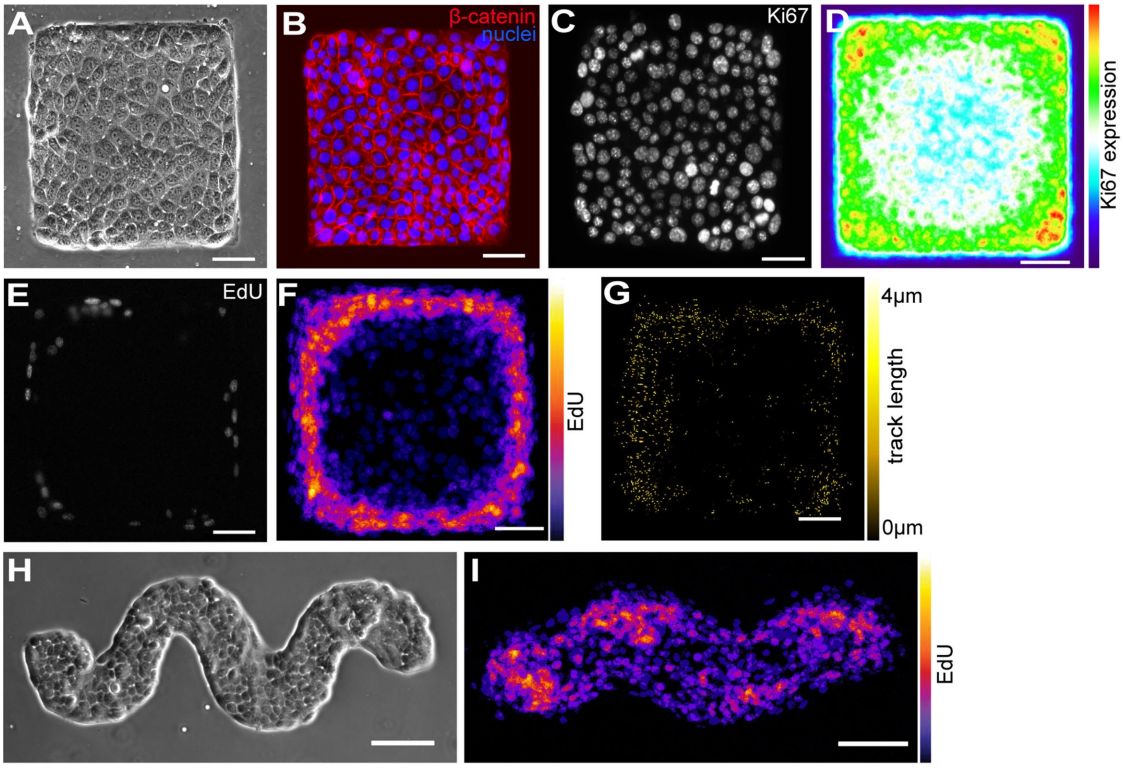

FIGURE 1: Microfabricated epithelial tissues exhibit patterns of proliferation defined by tissue geometry and mechanical stress. (A) Mammary epithelial cells were microfabricated into square tissues and (B) stained for nuclei and β-catenin. (C) Immunofluorescence analysis for Ki67 in an individual tissue and (D) frequency maps of 62 tissues ($n = 3$ independent replicates) reveal increased proliferation at the tissue periphery. (E) EdU analysis of an individual tissue and (F) frequency maps of 70 tissues ($n = 3$ independent replicates) show elevated synthesis of DNA at the periphery. (G) Traction force microscopy analysis shows increased mechanical stress at the periphery of the tissue ($n = 3$ separate tissues). (H) Phase-contrast image and (I) EdU frequency map of 16 sinusoidal tissues that contain both convex and concave regions. Scale bars represent 100 μm (H, I) or 50 μm (all other panels).

failed to establish a gradient of Vm across their geometry (Figure 4B). In contrast, tissues comprised of the negative control GFP-expressing cells established a gradient of Vm as expected (Figure 4, C and D). These trends persisted across multiple tissues (Figure 4, E and F). Furthermore, treating mammary epithelial tissues with the myosin II ATPase inhibitor blebbistatin (Kovács *et al.*, 2004) caused a significant reduction in the Vm gradient as compared to vehicle-treated controls (Figure 4, G–I). Intercellular transmission of cytoskeletal tension is thus required to establish a bioelectrical gradient across mammary epithelial tissues.

That transmission of mechanical force is necessary for the patterning of Vm suggested the possible involvement of tension-activated ion channels. The mechanosensitive ion channels Piezo1/2 open in response to mechanical forces from stretch or compression, permitting the influx of cations (Coste *et al.*, 2010; Wu *et al.*, 2016). We hypothesized that mechanical stress gradients that form across epithelial monolayers could result in patterned activation of Piezo1/2, leading to depolarization of cells located at the tissue periphery. Consistently, immunofluorescence analysis revealed increased expression of Piezo1 in cells located at the periphery of the tissues (Supplemental Figure S3, A–C). In contrast, we found that E_{null} tissues exhibited spatially uniform expression of Piezo1 (Supplemental Figure S3, D and E), suggesting a mechanical regulation of Piezo1 expression.

Changes in Piezo1 expression can affect the nuclear localization of Yap/Taz (Pathak *et al.*, 2014), important components of the Hippo pathway, which regulates organ size, proliferation, and apoptosis (Halder and Johnson, 2011). Specifically, Piezo1 knockdown was previously found to induce nuclear exclusion of Yap/Taz (Pathak *et al.*, 2014). In addition, mechanical stress gradients created by tissue geometry have been found to impact the nuclear localization of Yap/Taz (Aragona *et al.*, 2013). We therefore hypothesized that Yap/Taz would be excluded from nuclei in cells located in low-stress central regions of mammary epithelial tissues, where we observe decreased Piezo1 expression. As predicted, immunofluorescence analysis revealed increased nuclear localization of Yap/Taz in cells at the periphery of mammary epithelial tissues and nuclear exclusion within those at the center of the tissues (Figure 5, A–D). Consistent with a role for mechanical force, E_{null} tissues showed uniform nuclear localization of Yap/Taz across the entire tissue (Figure 5E). These data suggest that patterns of mechanical stress are required to generate the spatial pattern of Yap/Taz nuclear localization in this system. To determine whether Yap/Taz nuclear localization depends on depolarization, we examined Yap/Taz in tissues treated with gramicidin, which induces depolarization uniformly across the tissues. Consistently, the spatial pattern of Yap/Taz nuclear localization was attenuated in gramicidin-treated tissues (Figure 5, F–H), which showed increased nuclear localization of Yap/Taz in the cells in the center of the tissues as compared with untreated controls (Figure 5I). Our data suggest that depolarization of cells in regions of high mechanical stress leads to nuclear localization of Yap/Taz, which enhances proliferation in these regions of the tissue.

Yap/Taz play a significant role in the mechanical regulation of proliferation (Dupont *et al.*, 2011). We hypothesized that the nuclear localization of Yap/Taz in cells at the tissue periphery occurs

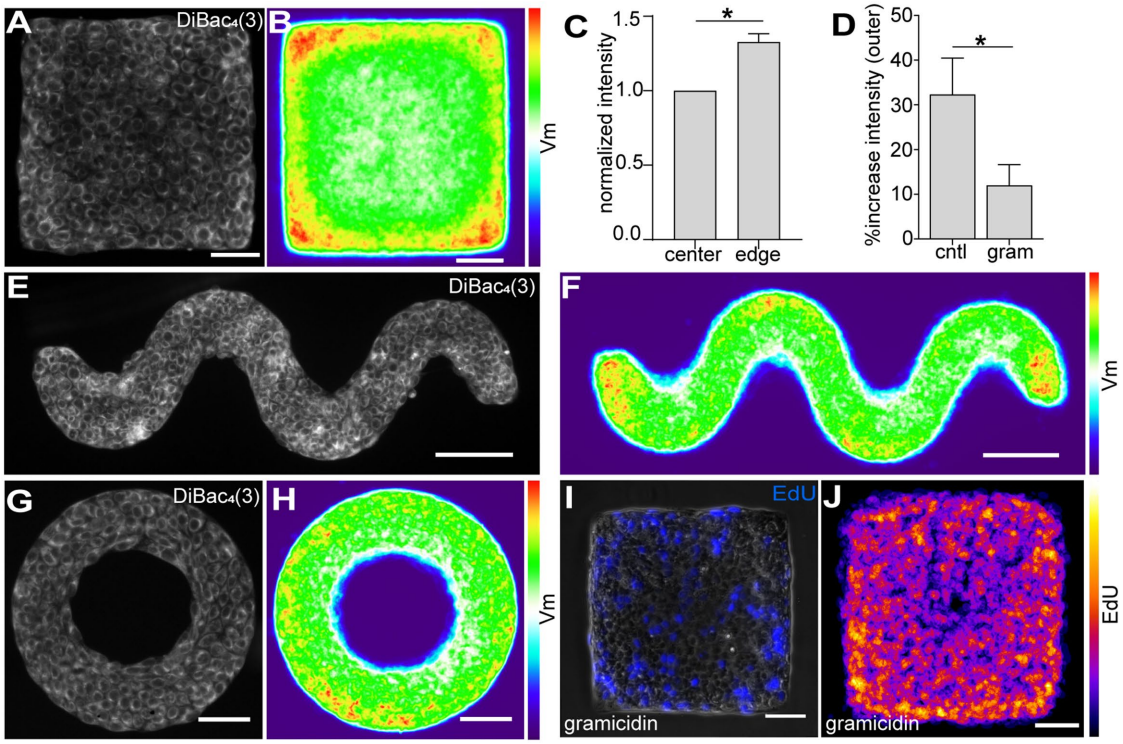

FIGURE 2: Cells located in high-stress regions show increased depolarization. (A) $DiBac_4(3)$ staining of a single square mammary epithelial tissue. (B) Frequency map of 78 tissues stained for $DiBac_4(3)$ across three independent replicates. Scale bars represent 50 μm. (C) Quantification of $DiBac_4(3)$ fluorescence in different regions of mammary epithelial tissues ($n = 3$ independent replicates). Shown are mean + SD. *$P < 0.05$ as determined by a one-sample *t* test comparing to a hypothetical value of one. (D) The percentage of difference in $DiBac_4(3)$ intensity between cells located in central and peripheral regions of control tissues compared with gramicidin-treated tissues ($n = 3$ independent replicates). Shown are mean + SD. *$P < 0.05$ as determined by an unpaired parametric *t* test with Welch's correction. (E) $DiBac_4(3)$ staining of a single sinusoidal tissue. (F) Frequency map of 21 sinusoidal tissues across a representative replicate. Scale bars represent 100 μm. (G) $DiBac_4(3)$ staining of a single annular tissue. (H) Frequency map of 23 annular tissues across a representative replicate. (I) Representative image of mammary epithelial tissues treated with gramicidin showing the location of EdU-positive cells (blue). (J) Frequency map of 78 tissues across three independent replicates reveals proliferation throughout the tissues. Scale bars represent 50 μm.

downstream of Vm and is required to establish the proliferation gradient across the tissue. Blocking Yap/Taz with verteporfin, which increases the levels of the 14-3-3σ chaperone protein and thereby sequesters Yap/Taz in the cytoplasm (Wang *et al.*, 2016), substantially decreased the expression of the Yap targets *ankrd1*, *birc5*, and *ctgf* (Figure 5J). As predicted, verteporfin had no effect on the Vm gradient (Figure 5K). However, verteporfin abolished proliferation in the tissues (Figure 5L), consistent with previous documentation of the antiproliferative effects of Yap inhibition (Wang *et al.*, 2016; Dasari *et al.*, 2017).

Enhanced expression of Piezo1 at the tissue periphery might indicate a heightened ion flux in response to mechanical force, which could play a role in establishing the Vm gradient. To test this hypothesis, we blocked Piezo1 with $GdCl_3$, a broad-spectrum inhibitor of mechanosensitive ion channels (Ermakov *et al.*, 2010). Surprisingly, we observed no effect on the Vm gradient (Figure 6A), which suggests that Piezo1 is not involved in its establishment. We therefore pursued alternate targets. Gap junctions permit the intercellular transfer of ions, thus establishing a tissue-scale bioelectric gradient by propagating changes in Vm between cells in a contact-dependent manner (Chernet *et al.*, 2015; Mathews and Levin, 2017). Treating tissues with carbenoxolone disodium (Sagar and Larson, 2006) blocked gap junctions, as demonstrated by a Lucifer Yellow dye-transfer assay (Supplemental Figure S4). Furthermore, treating mammary epithelial tissues with carbenoxolone also significantly attenuated the gradient in Vm (Figure 6, B and C). We therefore asked whether gap junctions are differentially regulated within the epithelial tissues. Gap junction activity can be measured using fluorescence recovery after photobleaching (FRAP) in combination with the cell-permeable dye calcein-AM. Once inside the cell, this dye is converted to a nonpermeable photoactive form that can be transported by gap junctions (Kuzma-Kuzniarska *et al.*, 2016). Photobleaching whole cells followed by measuring FRAP of calcein thus permits the visualization of gap junction activity (Gap-FRAP). Using this assay, we found that cells located at the tissue periphery showed similar FRAP dynamics to those located in the center (Supplemental Figure S5), indicating that gap junctions are not differentially regulated within the epithelial tissues.

Carbenoxolone not only inhibits gap junctions but also blocks pannexin channels and connexin hemichannels (Verselis and Srinivas, 2013). The promiscuity of this inhibitor is relevant, since pannexin1 and Cx43 hemichannels can also be gated mechanically (Bao *et al.*, 2004; Cherian *et al.*, 2005; Batra *et al.*, 2012). To investigate the possible role of pannexin and connexin hemichannels, we labeled tissues with the cationic vital dyes YoPro and propidium iodide (PI), which have been used to visualize pannexin and connexin hemichannel function in nonapoptotic cells (Patel *et al.*, 2014). We observed uptake of both of these dyes primarily in cells at the periphery of the control tissues

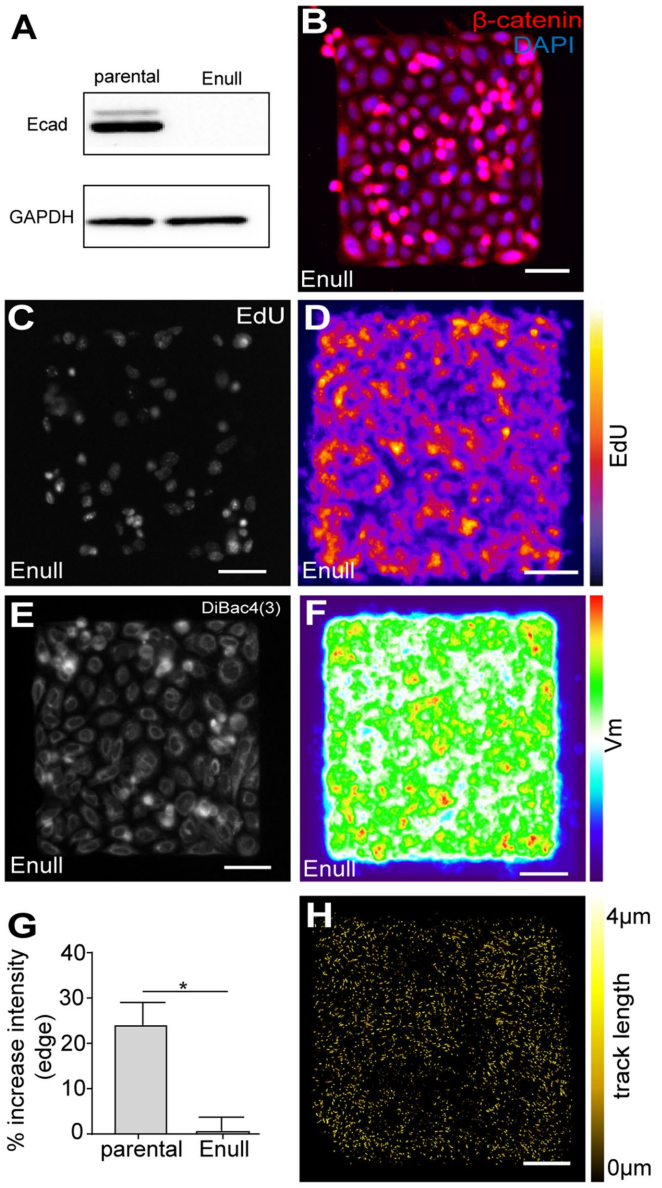

FIGURE 3: Gradients of Vm and proliferation require intercellular contacts. (A) Immunoblotting analysis for E-cadherin (Ecad) and GAPDH in parental mammary epithelial and E_{null} cells ($n = 3$). (B) E_{null} cells were microfabricated into square tissues and stained for nuclei and β-catenin. (C) EdU analysis of an individual E_{null} tissue and (D) frequency maps of 25 tissues across a representative replicate reveal a uniform pattern of DNA synthesis. (E) $DiBac_4(3)$ staining of an individual E_{null} tissue and (F) frequency map of 27 tissues across a representative replicate. (G) Quantification of $DiBac_4(3)$ fluorescence in different regions of E_{null} tissues ($n = 3$ independent replicates). Shown are mean + SD. $^*P < 0.05$ as determined by an unpaired parametric *t* test with Welch's correction. (H) Traction force microscopy of E_{null} tissues ($n = 3$) revealed no discernable pattern of mechanical stress within the tissue. Scale bars represent 50 μm.

(Figure 6D), but not in tissues comprised of E_{null} cells (Figure 6E) or in the concave regions of sinusoidal tissues (Figure 6F) that experience low mechanical stress. We observed very few cells that expressed cleaved caspase-3 (Figure 6G) or showed DNA damage (Figure 6H) within control tissues, indicating that the YoPro/PI signals we observed were not simply due to apoptosis. These data suggest that endogenous mechanical stresses activate pannexin channels and/or connexin hemichannels in mammary epithelial tissues.

We therefore took advantage of specific inhibitors of each. We found that treating tissues with the pannexin1 inhibitor ^{10}Panx had no effect on the Vm gradient (Figure 7A). However, treatment with the peptide TAT-gap19, which specifically inhibits Cx43 hemichannels but has no effect on gap junctions (Abudara *et al.*, 2014), significantly reduced the uptake of YoPro dye in cells located in high-stress regions (Figure 7, B and C). These tissues also failed to establish gradients of Vm (Figure 7, D and E). Additionally, treatment with TAT-gap19 significantly attenuated the number of proliferating cells at the periphery of epithelial tissues (Figure 7, F–H). As expected, we also found a reduction in the gradient of Yap/Taz nuclear localization in tissues treated with TAT-gap19 (Figure 7, I and J). Immunofluorescence analysis for Cx43 protein revealed localization at cell–cell junctions consistent with gap junctions as well as puncta at the apical surface (Figure 7, K and L), as might be expected for hemichannels (Patel *et al.*, 2014). Together, these data suggest that mechanical gating of Cx43 hemichannels promotes depolarization in cells at the periphery of epithelial tissues, leading to Yap/Taz activation and enhanced proliferation in these regions.

We observed patterns of depolarization approximately 24–48 h before the pattern of proliferation emerged in the tissues, consistent with our hypothesis that changes in the gradient of Vm templates the proliferation pattern. However, increased depolarization has been observed to coincide with the G2/M phase of the cell cycle (Yang and Brackenbury, 2013) and, therefore, depolarization at the tissue periphery could also result from the increase in proliferation in this region. To determine whether proliferation causes depolarization, we inhibited cell-cycle progression in mammary epithelial tissues by treating with aphidicolin (Huberman, 1981; Lalande, 1990) or mitomycin C (Kang *et al.*, 2001; Zhou *et al.*, 2011) (Supplemental Figure S6A). Both of these treatments completely abolished proliferation in the tissues, but neither impacted the spatial pattern of Vm (Supplemental Figure S6, B and C). These data confirm that the Vm gradient is upstream of the proliferation gradient in mammary epithelial tissues.

DISCUSSION

Here, we found that patterns of mechanical stress resulting from the geometry of epithelial tissues induce patterns of depolarization that presage patterns of proliferation. Buildup of mechanical tension across the epithelial monolayer is not only merely coordinated with but also required for the formation of this Vm gradient. Thus, the geometry of the tissue defines the pattern of Vm that forms across an epithelial sheet. Consistently, we observed a spatial gradient in the nuclear localization of Yap/Taz across the tissues that correlates with the pattern of mechanical stress. The Vm gradient is required for the formation of the pattern of nuclear Yap/Taz. These results are consistent with the fact that Yap/Taz shuttles into the nucleus in response to mechanical stimuli, including stretch, compression, and substratum stiffness (Aragona *et al.*, 2013). However, our data suggest that mechanical stress signals through Vm to regulate Yap/Taz.

There are several mechanisms by which mechanical stress can induce changes in Vm. Piezo1 has been implicated in the transduction of mechanical signals into changes in ion flow in various biological contexts (Coste *et al.*, 2010). However, we found that inhibiting Piezo1 had no effect on the Vm gradient in mammary epithelial tissues. Our data instead suggest that mechanical stress regulates Vm by altering ion flow through Cx43 hemichannels. The Vm gradient across the tissues is abolished in the presence of the peptide TAT-gap19, a specific blocker of Cx43 hemichannels. Consistently, we observed a pattern of YoPro and PI dye uptake in cells

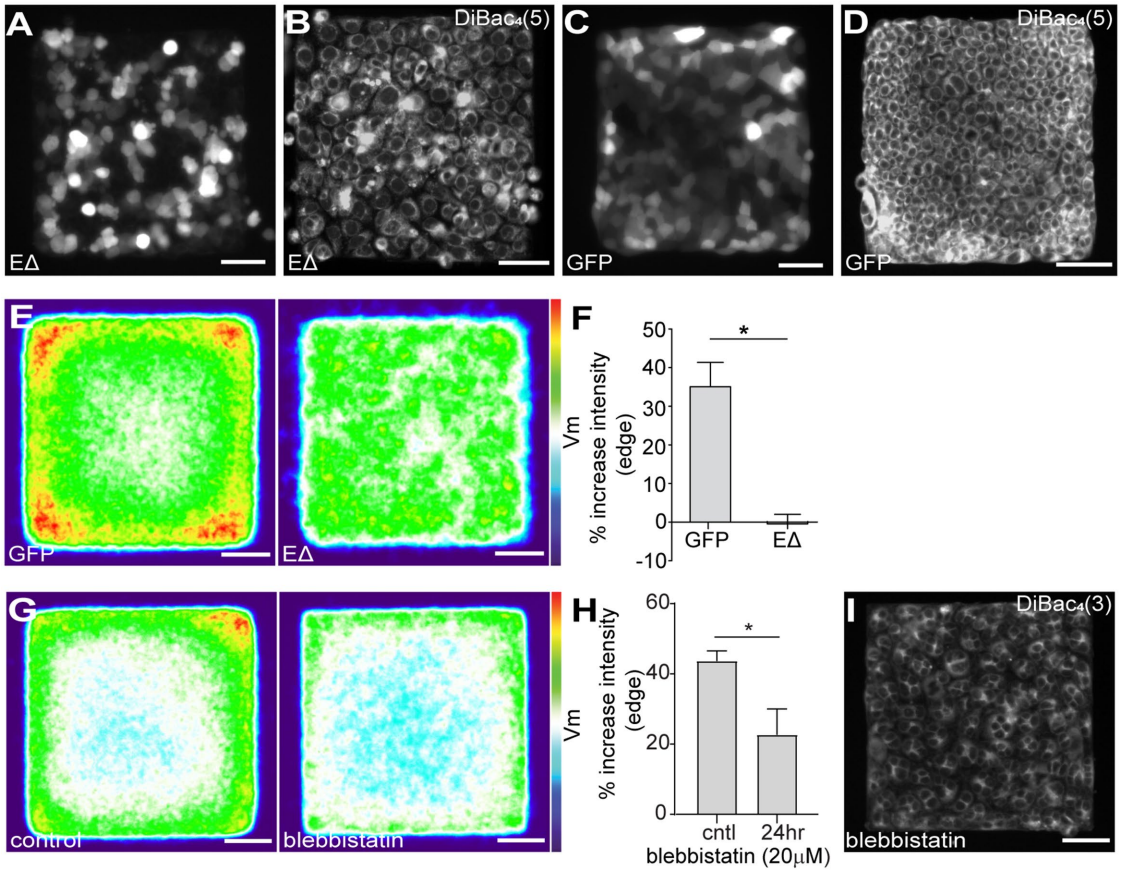

FIGURE 4: Gradients of Vm and proliferation depend on intercellular transmission of force. (A) GFP expression in a tissue transduced with bicistronic adenovirus encoding for GFP and EΔ. (B) $DiBac_4(5)$ staining of an individual EΔ tissue. (C) GFP expression in a tissue transduced with control adenovirus encoding GFP alone. (D) $DiBac_4(5)$ staining of an individual GFP control tissue. (E) Frequency map of 45 GFP control tissues (left) and 41 EΔ tissues (right) stained with $DiBac_4(5)$. (F) Quantification of $DiBac_4(5)$ fluorescence in different regions of Ad-GFP or EΔ tissues. (G) Frequency map of 50 control tissues (left) and 55 blebbistatin-treated tissues (right) treated with $DiBac_4(3)$. (H) Quantification of $DiBac_4(3)$ fluorescence in different regions of control or blebbistatin-treated tissues. (I) $DiBac_4(3)$ imaging in an epithelial tissue treated with blebbistatin. Three independent replicates were performed for all experiments. Shown are mean + SD. *$P < 0.05$ as determined by an unpaired parametric *t* test with Welch's correction. Scale bars represent 50 μm.

located in high-stress regions of the tissues that was significantly attenuated on treatment with TAT-gap19. Cx43 hemichannels have been previously documented to be opened by mechanical stress via a direct connection to α5β1 integrin (Batra *et al.*, 2012). It is therefore possible that enhanced integrin signaling in the high-stress regions of the mammary epithelial tissues also regulates Cx43 hemichannels.

Hemichannels can be gated by Ca^{2+} (Lopez *et al.*, 2016), which has been shown to signal downstream of mechanical stress (Sjaastad *et al.*, 1996; Kwon *et al.*, 2000; Ohata *et al.*, 2001; Alenghat *et al.*, 2004). Furthermore, depolarization can affect levels of intracellular Ca^{2+} through voltage-gated calcium channels (Catterall, 2011), and intracellular Ca^{2+} can influence the nuclear translocation of Yap (He *et al.*, 2018; Liu *et al.*, 2019). It was therefore plausible that intracellular Ca^{2+} played a role in the mechanical regulation of Vm by Cx43 hemichannels or in trafficking of Yap/Taz downstream of Vm signals in the mammary epithelial tissues. Consistently, we observed an increase in intracellular Ca^{2+} in cells located in regions of high mechanical stress (Supplemental Figure S7A). Abolishing this gradient by chelating intracellular Ca^{2+} (Supplemental Figure S7, B and C) attenuated the spatial pattern of nuclear Yap (Supplemental Figure S7, D and E) and proliferation (Supplemental Figure S7, F and G), but had no effect on the pattern of uptake of YoPro dye (Supplemental Figure S7H), suggesting that Ca^{2+} does not regulate hemichannels in these tissues. However, chelating intracellular Ca^{2+} abolished the gradient of membrane depolarization in the tissues (Supplemental Figure S7, I and J). Ca^{2+} is required for E-cadherin function (Ozawa *et al.*, 1990) and intricately involved in mechanosensation. However, we did not observe mislocalization of E-cadherin or β-catenin in tissues chelated of intracellular Ca^{2+} (Supplemental Figure S7, K and L), suggesting that Ca^{2+} exerts its effects on Vm downstream of mechanical stress. Conversely, blocking hemichannels had no effect on the level or gradient of intracellular Ca^{2+} (Supplemental Figure S7, M and N), suggesting that hemichannels signal independently of Ca^{2+} to regulate nuclear localization of Yap and proliferation. We conclude that intracellular Ca^{2+} neither regulates hemichannels downstream of mechanical stress nor serves as a mediator between depolarization and Yap localization in these epithelial tissues. However, sufficient intracellular Ca^{2+} levels are required for mechanical stress to influence Vm and downstream signaling.

Our results thus suggest a model that links mechanical stress gradients to membrane depolarization. Contraction of neighboring cells in epithelial tissues leads to the emergence of mechanical stress gradients that depend on tissue geometry (Figure 8). Cx43 hemichannels

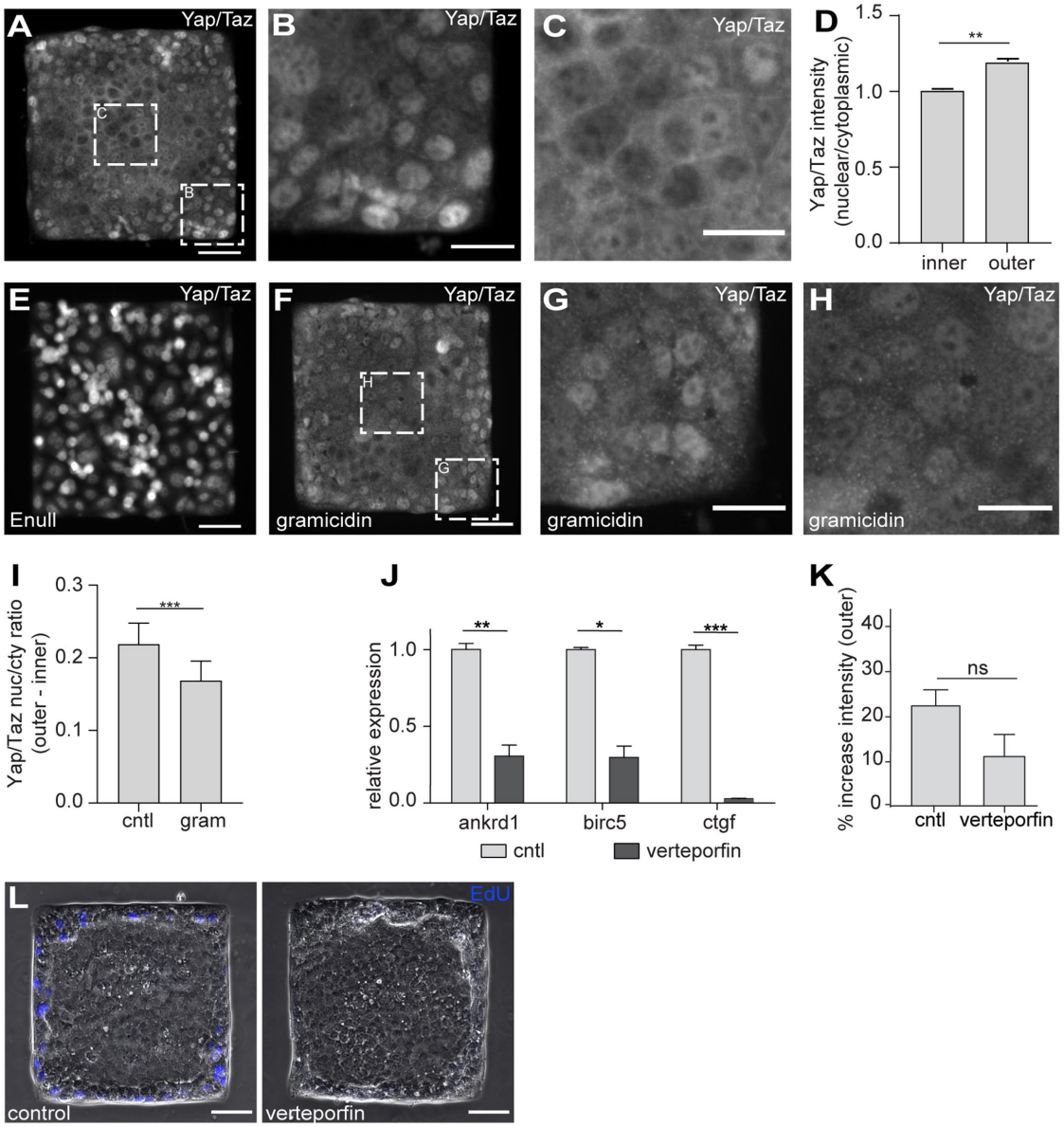

FIGURE 5: Tissue geometry and Vm regulate spatial patterns of Yap/Taz nuclear localization. (A) Immunofluorescence analysis for Yap/Taz in a representative mammary epithelial tissue. Scale bar represents 50 μm. (B) Magnified image of the area indicated by the dashed white line in A, showing increased nuclear localization of Yap/Taz in cells at the tissue periphery. (C) Magnified image of the center of the tissue shown in A. Scale bars represent 25 μm. (D) Quantification of Yap/Taz nuclear/cytoplasmic ratios in cells located in different regions of the tissues ($n = 3$ independent replicates). Shown are mean + SD. $^{**}P < 0.01$ as determined by an unpaired parametric *t* test with Welch's correction. (E) Immunofluorescence analysis for Yap/Taz in a representative E_{null} tissue. Scale bar represents 50 μm. (F) Immunofluorescence analysis for Yap/Taz in a mammary epithelial tissue depolarized by treatment with gramicidin. Scale bar represents 50 μm. (G) Magnified image of the area indicated by the dashed white line in F, showing Yap/Taz in cells at the tissue periphery. (H) Magnified image of the center of the tissue shown in F. Scale bars represent 25 μm. (I) Difference in nuclear/cytoplasmic ratio of Yap/Taz immunofluorescence in outer and inner cells of tissues treated with gramicidin vs. control ($n = 3$ independent replicates). Shown are mean + SD. $^{***}P < 0.001$ as determined by a paired parametric *t* test. (J) RT-qPCR showing transcript levels of the Yap targets *ankrd1, birc5,* and *ctgf* on treatment with verteporfin (3 μM; $n = 3$ independent replicates). Shown are mean + SD. $^{*}P < 0.05$; $^{**}P < 0.01$; $^{***}P < 0.001$, as determined by an unpaired parametric t-test with Welch's correction. (K) Quantification of $DiBac_4(3)$ fluorescence difference in inner vs. outer regions of verteporfin-treated tissues ($n = 3$ independent replicates). Shown are mean + SD. (L) Representative images of EdU-positive cells (blue) in control or verteporfin-treated tissues. Scale bars represent 50 μm.

open in response to mechanical stress, allowing membrane depolarization of cells in high-stress regions. Membrane depolarization promotes the nuclear localization of Yap, which induces proliferation. It will be interesting to determine how mechanical stress gradients in other microenvironmental scenarios, including three-dimensional epithelial tissues (Gjorevski and Nelson, 2012), regulate Vm.

The molecular mechanisms through which membrane depolarization affect the nuclear trafficking of Yap/Taz remain unclear. A

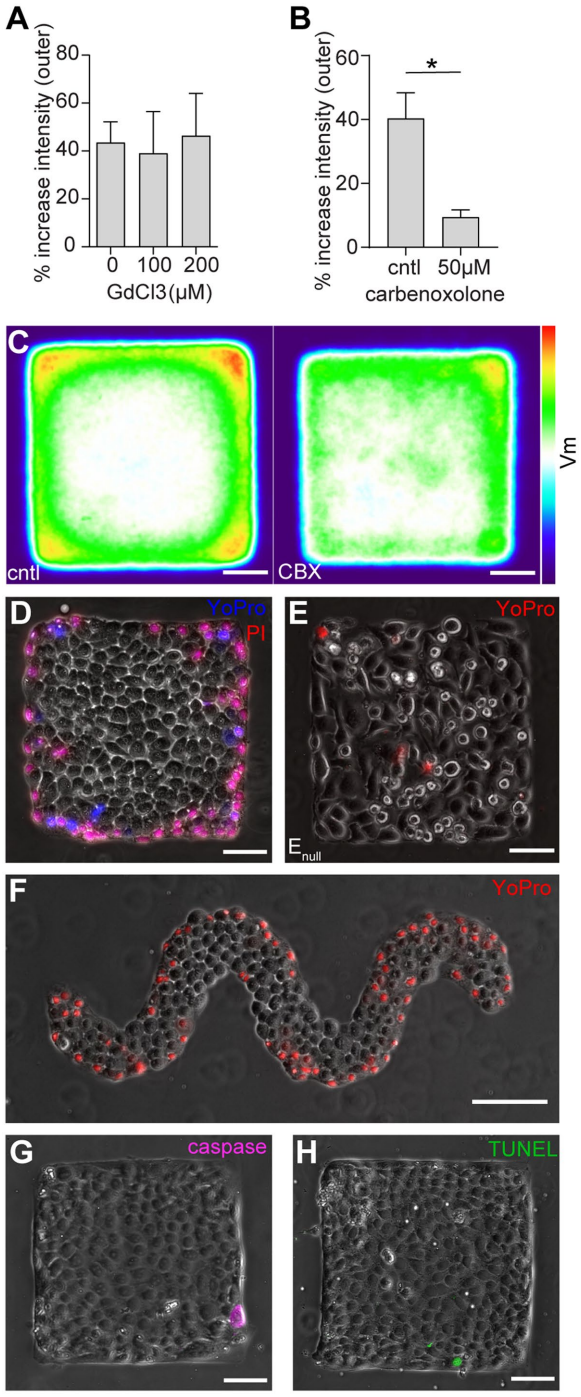

FIGURE 6: Large-diameter ion conduits are implicated in the regulation of Vm by tissue geometry. (A) Quantification of $DiBac_4(3)$ fluorescence in different regions of tissues treated with $GdCl_3$ ($n = 3$ independent replicates). Shown are mean + SD. (B) Quantification of $DiBac_4(3)$ fluorescence in different regions of tissues treated with carbenoxolone (CBX). Shown are mean +SD. *$P < 0.05$ as determined by an unpaired parametric *t* test with Welch's correction ($n = 3$ independent replicates). (C) Frequency map of $DiBac_4(3)$ fluorescence in 85 control tissues (left) and 93 CBX-treated tissues (right) across three independent replicates. (D) Representative images of YoPro or PI uptake in epithelial tissues (red, PI; blue, YoPro; gray, phase contrast). (E) Representative image of YoPro uptake in an E_{null} tissue (red, YoPro; gray, phase contrast). Scale bars represent 50 μm. (F) Representative image of YoPro uptake in a sinusoidal epithelial tissue (red, YoPro; gray, phase contrast). Scale bar represents 100 μm. (G) Representative image of cleaved caspase-3 immunofluorescence in an epithelial tissue (magenta, caspase-3; gray, phase contrast). (H) Representative image of TUNEL assay in an epithelial tissue (green, TUNEL; gray, phase contrast). Scale bars represent 50 μm.

genomewide microarray analysis of transcriptome changes in response to depolarization revealed that more than 2700 genes were up- or down-regulated in human mesenchymal stem cells, including the Hippo signaling components Lats2, Tead2, and Tead4 (Pai *et al.*, 2016; Holden and Cunningham, 2018). The large number of genes regulated in response to depolarization suggests that multiple pathways and feedback loops may interact to generate downstream phenotypes. Increased cytosolic levels of Ca^{2+} have also been implicated in nuclear trafficking. Vm has been documented to control dopamine transporter trafficking between the plasma membrane and endosomes in a manner dependent on Ca^{2+}/calmodulin-dependent protein kinase II (CaMKII) (Richardson *et al.*, 2016). In this mechanism, membrane depolarization increases levels of cytosolic Ca^{2+} leading to increased activation of CaMKII. This kinase is also involved in noncanonical Wnt signaling, which is proposed to interact with the Hippo pathway and impact Yap translocation via interactions with the β-catenin/Scribble complex (Bernascone and Martin-Belmonte, 2013). More studies of the cross-talk in signaling pathways and transcriptome changes in response to Vm manipulation in additional cell types are needed to fully understand the underlying mechanisms.

MATERIALS AND METHODS

Cell culture

EpH4 mouse mammary epithelial cells (ATCC) were maintained in 1:1 DMEM:F12 (ThermoFisher Scientific) supplemented with 2% heat-inactivated fetal bovine serum (FBS; Atlanta Biologicals), 50 μg/ml gentamicin (Life Technologies), and 5 μg/ml insulin (Sigma); cells were confirmed to be free of mycoplasma using a commercially available kit (Lonza). Cell–cell adhesions were manipulated by Crispr/Cas9-mediated deletion of E-cadherin (E_{null}). To knock out E-cadherin, EpH4 cells were transfected with a commercially available CRISPR/Cas9 kit targeting murine *CDH1*. Specifically, cells were transfected either with plasmid encoding the Cas9 nuclease and a 20-nucleotide guide RNA targeting *CDH1* (sc-419587, Santa Cruz, Dallas, TX) or control CRISPR/Cas9 plasmid (sc-418922, Santa Cruz) coexpressing GFP. Single, GFP-positive cells were sorted into a 96-well plate using BD FACSVantage SE w/DiVa (BD Biosciences) 48 h after transfection. Knockout efficiency was assessed by immunoblotting, as described previously (Pang *et al.*, 2016). Intercellular transmission of mechanical stress was inhibited by transducing cells with recombinant adenovirus that encoded for an E-cadherin mutant lacking the amino-terminal β-catenin-binding domain (EΔ) (Gjorevski and Nelson, 2010; Gomez *et al.*, 2010; Piotrowski-Daspit *et al.*, 2016, 2017). As a negative control, cells were transduced with adenovirus that encoded for GFP. Virus was added to achieve transduction efficiency of at least 99%. The Vm gradient was abolished by applying gramicidin (1 μg/ml; Sigma) for 24 h prior to analysis of Vm or proliferation. Gramicidin is a 15-amino acid polypeptide that inserts into the plasma membrane and forms conduits for ion flow (Wallace, 1990). This drug depolarizes cells (Maric *et al.*, 1998; Klapperstuck *et al.*, 2013) by allowing the free passage of monovalent cations through gramicidin channels (Wallace, 1990; Kelkar and Chattopadhyay, 2007), disrupting the ability of cells to maintain a hyperpolarized state and regulate their own Vm.

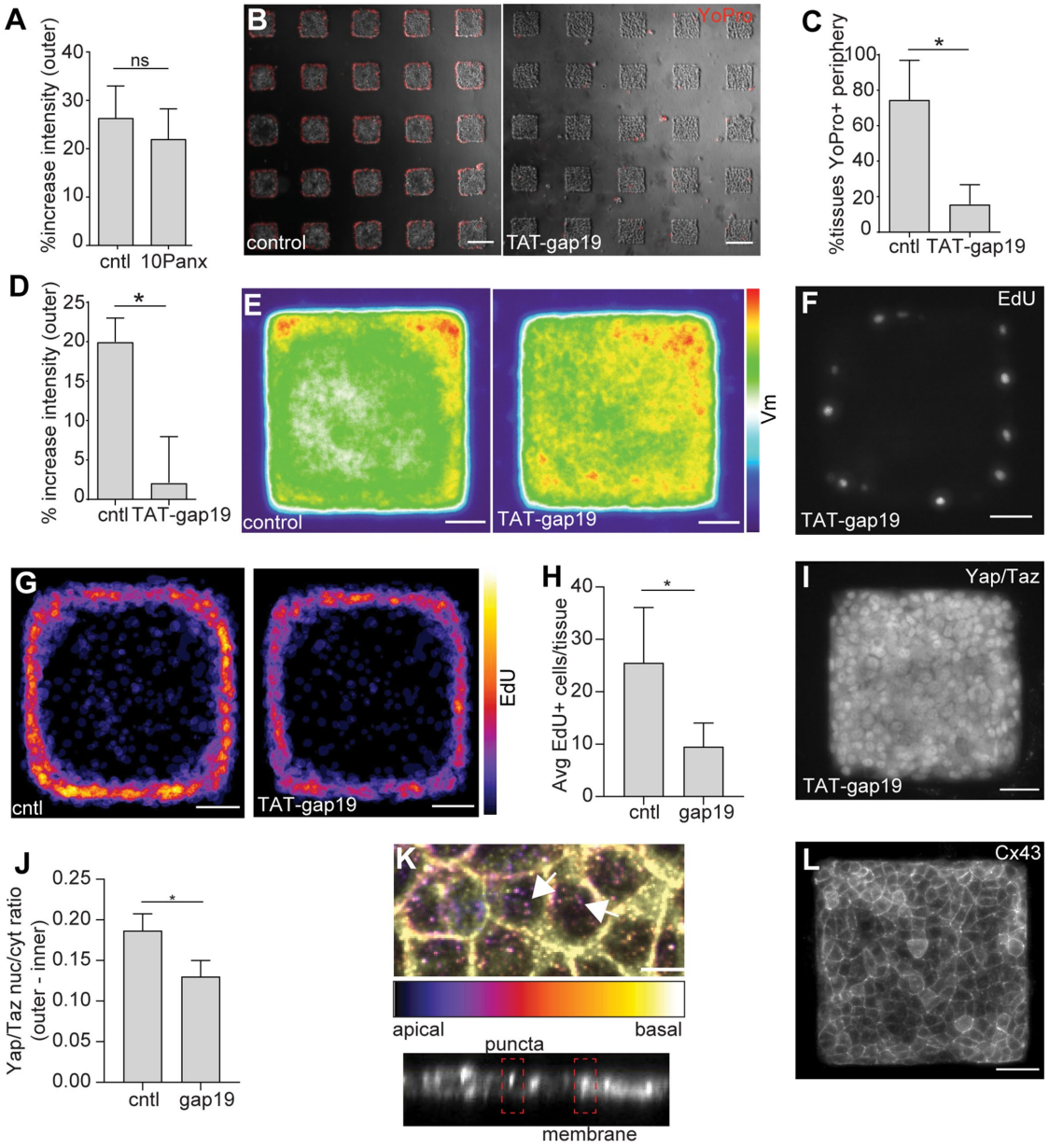

FIGURE 7: Cx43 hemichannels are required for spatial gradients of Vm. (A) Quantification of $DiBac_4(3)$ fluorescence in different regions of tissues treated with 10Panx ($n = 3$ independent replicates). Shown are mean + SD. (B) Representative image of YoPro uptake in tissues treated with TAT-gap19. (C) Percentage of tissues showing YoPro uptake at the periphery ($n = 3$ independent replicates). Shown are mean + SD. *$P < 0.05$ as determined by an unpaired Student's t test ($n = 3$ independent replicates (D) Quantification of $DiBac_4(3)$ fluorescence in different regions of tissues treated with TAT-gap19. Shown are mean + SD. *$P < 0.05$ as determined by an unpaired parametric t test with Welch's correction. (E) Frequency map of $DiBac_4(3)$ fluorescence in 24 control tissues (left) and 23 TAT-gap19-treated tissues (right) across a representative replicate. (F) EdU analysis of a representative tissue treated with TAT-gap19. (G) Frequency maps of 66 control tissues (left) and 75 tissues treated with TAT-gap19 (right) across three independent replicates show a qualitative decrease in average EdU signal at the periphery of the tissues. (H) Quantification of number of EdU-positive cells at the periphery of tissues treated with TAT-gap19 vs. control ($n = 3$ independent replicates). Shown are mean + SD. *$P < 0.05$ as determined by an unpaired Student's t test with Welch's correction. (I) Immunofluorescence analysis for Yap/Taz in an individual TAT-gap19-treated tissue. (J) Quantification of the difference in Yap/Taz nuclear/cytoplasmic ratio in outer vs. inner cells of tissues treated with TAT-gap19 ($n = 3$ independent replicates). Shown are mean + SD. *$P < 0.05$ as determined by an unpaired Student's t test with Welch's correction. (K) Immunofluorescence analysis for Cx43 in epithelial tissues showing lateral membrane localization (gap junctions) and apical puncta (putative hemichannels). (L) Immunofluorescence analysis for Cx43 across an entire epithelial tissue. Scale bars represent 10 μm (K) or 50 μm (all other panels).

Intracellular Ca^{2+} chelation was performed by applying BAPTA-AM (10 μM, 24 h; Thermo Fisher Scientific). Yap/Taz activity was inhibited using verteporfin (3 μM, 24 h; Thermo Fisher Scientific). Proliferation was inhibited using either mitomycin C (2.5 μg/ml; Thermo Fisher Scientific) or aphidicolin (0.5 μg/ml; Thermo Fisher Scientific). Piezo1 channels were inhibited using $GdCl_3$ (100, 200 μM;

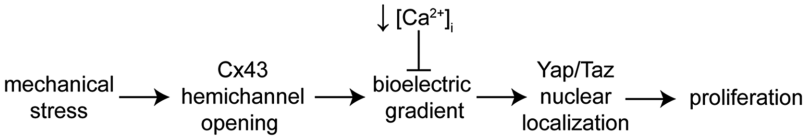

FIGURE 8: Proposed model for the regulation of Vm gradients by epithelial tissue geometry. Mechanical stress at the tissue periphery triggers opening of Cx43 hemichannels, causing membrane depolarization. This in turn facilitates Yap/Taz localization to the nucleus in a calcium-dependent manner, increasing proliferation at the tissue periphery.

Alfa Aesar). Pannexin1 channels were inhibited using ^{10}Panx (200 μM; Tocris). Cx43 hemichannels were inhibited using the peptide TAT-gap19 (Abudara *et al.*, 2014) (50 μM, 20 h; Tocris). Cytoskeletal tension was inhibited using blebbistatin (20 μM, 24 h; Sigma Aldrich).

Micropatterned tissues

Islands of fibronectin were generated by microcontact printing as described previously (Tan *et al.*, 2004). Cells were seeded onto the fibronectin islands at a density of approximately 1.4×10^3 cells/mm^2 for 2–3 h. Nonadherent cells were removed by washing once with culture medium. Adherent cells were cultured for approximately 24 h on the islands, until confluent. For EdU analysis, tissues were cultured for a total of 72 h.

Immunofluorescence analysis and proliferation assays

Samples were fixed with 4% paraformaldehyde in phosphate-buffered saline (PBS) for 20 min at room temperature. Fixative was removed by washing three times for 5–10 min in PBS, followed by washing three times in 0.3% Triton X-100 (Sigma Aldrich) in PBS (PBST). Samples were blocked in 10% (vol/vol) goat serum (Sigma Aldrich) in PBST for 1 h, then incubated overnight at 4°C with primary antibodies to label E-cadherin (Abcam), beta-catenin (Abcam), Ki67 (Abcam), Yap/Taz (Cell Signaling), Cx43 (Cell Signaling), cleaved caspase-3 (Cell Signaling), or Piezo1 (Novus). Following incubation with primary antibody, samples were washed three times in PBST, then incubated with Alexa 594–conjugated goat anti-rabbit secondary antibody (Invitrogen) overnight at 4°C. Prior to imaging, samples were washed three times in PBS. Nuclei were visualized by incubating the cells for 15 min in Hoechst 33342 diluted 1:1000 in PBS, followed by three washes with PBS. To visualize proliferation, we used the Click-iT EdU Alexa Fluor 488 or 594 Imaging Kits (Thermo Fisher Scientific). Tissues were exposed to EdU-containing growth medium for 30 min prior to fixation and detection. To detect DNA damage, we used the Click-iT Plus TUNEL Assay for In Situ Apoptosis Detection (Thermo Fisher Scientific).

Voltage-reporter imaging, Ca^{2+} visualization, and dye-uptake assays

The voltage-reporter dyes $DiBac_4(3)$ or $DiBac_4(5)$ were used to visualize gradients of cellular Vm throughout the tissues. These dyes more easily enter the plasma membrane of depolarized (more positively charged) cells in a manner where each percentage of increase in fluorescence intensity is approximately linearly proportional to the millivolt change in Vm (Klapperstuck *et al.*, 2013). $DiBac_4(3)$ was applied at a concentration of 2 μg/ml in culture medium supplemented with 2% FBS and incubated for at least 30 min at 37°C before imaging at 488 nm. Live tissues were imaged at room temperature in the dye solution, which had a pH of 7.0–7.4.

To visualize intracellular Ca^{2+}, we applied Calcium Green 1 (CG1, 10 μM, 24 h; Thermo Fisher Scientific). Excess dye was removed by washing 3× in culture medium prior to imaging at 488 nm. To visualize vital dye uptake, we used YO-PRO-1 or PI (Thermo Fisher Scientific) diluted 1:1000 in PBS. Tissues were washed 3× in PBS before application of the dye. Samples were incubated in the dark at room temperature for 15 min prior to visualization.

Traction force analysis

Polyacrylamide gel substrata with a 300:1 acrylamide:bis-acrylamide ratio were prepared as described (Polio and Smith, 2014). Fluorescent beads (Invitrogen; FluoSpheres carboxylate, 500 nm, yellow-green 505/515 nm λ) were mixed into the bulk polyacrylamide gel. Fibronectin-printed glass coverslips as described above were added to the surface of the polyacrylamide mixture during gelation to promote transfer of protein to the gel surface. After removing the coverslip, the remaining NHS-ester (N-hydroxysuccinimide ester; Sigma-Aldrich) on the surface was passivated by incubating in a solution of 4% bovine serum albumin (Sigma-Aldrich) in PBS. After sterilization of the gels, cells were seeded on the fibronectin islands to form tissues and incubated for 72 h. Samples were imaged under phase-contrast and fluorescence microscopy before and after relaxation with 0.05% Trypsin-EDTA (Life Technologies). Bead positions were measured using ImageJ and Imaris (Bitplane).

Microscopy

All samples were imaged using a Nikon Eclipse Ti-U inverted fluorescence microscope (Nikon, Melville, NY) equipped with a Hamamatsu ORCA charge-coupled device camera (Hamamatsu, Japan). Images were taken at 488 or 594 nm using a 20× air objective. At least three biological replicates were included in each experiment, and at least 10 tissues were imaged per replicate. Background fluorescence was subtracted from the images prior to analysis. An average fluorescence distribution for each replicate was obtained by stacking the individual tissues in ImageJ using the average intensity z-projection function. The average fluorescence intensity was then determined by taking the mean fluorescence intensity value for the innermost (5–10 cells wide) and outermost (2–3 cells wide) regions of the stack using ImageJ. The outermost signal was normalized to the innermost signal by calculating the difference between the two intensity values and dividing by the fluorescence value for the innermost cells. This value was shown as the percentage increase in signal of the outermost to the innermost region. Frequency maps of relative Vm were obtained by creating average stacks of $DiBac_4(3)$ fluorescence intensity of the tissues for a representative replicate and converting to a color scale in ImageJ. Frequency maps of intracellular Ca^{2+} were similarly obtained by creating average stacks of CG1 fluorescence for each representative replicate. Frequency maps of Piezo1 immunofluorescence were created similarly. Frequency maps of EdU fluorescence were obtained by creating average stacks of thresholded fluorescence intensity of each replicate (n = 3), then summing these stacks and converting to a color scale in ImageJ.

Lucifer Yellow dye-transfer assay

Efficacy of the gap junction blocker carbenoxolone was visualized by transfer of Lucifer Yellow as previously described (Opsahl and Rivedal, 2000). Briefly, epithelial monolayers were wounded in the presence of 1.0% Lucifer Yellow (Thermo Fisher Scientific) in PBS. Tissues were incubated for 5 min at 37°C prior to visualization. Gap junctions were blocked using carbenoxolone disodium (50 μM; Sigma) applied 24 h prior to performing the assay. Plots of the fluorescence intensity as a function of distance from the scratch were created in ImageJ.

Gap-FRAP assay

Quantitative assessment of gap junction activity was performed using FRAP as previously described (Kuzma-Kuzniarska *et al*., 2016). Briefly, epithelial tissues were treated with calcein-AM (Thermo Fisher Scientific) for approximately 30 min, then excess dye was washed away using fresh culture medium. FRAP was performed on a Nikon A1R-Si HD confocal microscope. Whole cells were photobleached, then monitored for fluorescence recovery over a 4-min period. Recovery traces were plotted using minmax normalization. Cells in the center of the tissue ("inner") were compared with cells located one cell layer in from the periphery of the tissue ("outer"), to control for number of neighbors.

Patch clamp assay

Mammary epithelial cells plated on glass coverslips were treated with 2 µg/ml $DiBac_4(3)$ for at least 30 min prior to patch clamping. During recordings, cells were perfused at a flow rate of 4–5 ml/min with a recording ACSF solution (127 mM NaCl, 5 mM KCl, 25 mM HEPES, 1.2 mM $MgCl_2$, 2 mM $CaCl_2$, and 6 mM D-glucose, pH adjusted to 7.4 with NaOH). Whole-cell recordings were performed using a Multiclamp 700B (Molecular Devices, Sunnyvale, CA) using pipettes with a resistance of 3–5 MΩ filled with a potassium-based internal solution (140 mM KCl, 0.2 mM EGTA, 10 mM HEPES, 4 mM $MgCl_2$, and 5 mM Na-ATP, pH adjusted to 7.2 with KOH). A slow voltage ramp (2 mV/min) from –20 mV to +20 mV was applied to each of five cells and $DiBac_4(3)$ fluorescence recorded. Fluorescence of nonpatched cells in the same field-of-view was recorded and used as an internal control to correct for photobleaching of the dye.

Cell morphology analysis

Ten cells located at the periphery or center in each of four epithelial tissues stained for E-cadherin were outlined in ImageJ. Aspect ratio and circularity were calculated and compared for the cells in each location. To assess the impact of cell morphology on $DiBac_4(3)$ fluorescence, EpH4 cells were cultured on tissue culture polystyrene for 24 hr, then treated with $DiBac_4(3)$ for at least 20 min prior to imaging. Aspect ratio and circularity were calculated in ImageJ for 100 cells and plotted against $DiBac_4(3)$ fluorescence. Significance was determined based on calculation of Spearman correlation coefficients for each parameter.

ACKNOWLEDGMENTS

This work was supported in part by grants from the National Institutes of Health (CA187692, CA214292) and a Faculty Scholars Award from the Howard Hughes Medical Institute. B.B.S. was supported in part by the NSF Graduate Research Fellowship Program. J.L. thanks Samuel S.-H. Wang for support (NIH R01 MH115750).

REFERENCES

Abudara, V., Bechberger, J., Freitas-Andrade, M., De Bock, M., Wang, N., Bultynck, G., Naus, C.C., Leybaert, L., Giaume, C. (2014). The connexin43 mimetic peptide Gap19 inhibits hemichannels without altering gap junctional communication in astrocytes. Front Cell Neurosci 8, 306.

Adams, D.S., Levin, M. (2013). Endogenous voltage gradients as mediators of cell-cell communication: strategies for investigating bioelectrical signals during pattern formation. Cell Tissue Res 352, 95–122.

Adams, D.S., Masi, A., Levin, M. (2007). H+ pump-dependent changes in membrane voltage are an early mechanism necessary and sufficient to induce Xenopus tail regeneration. Development 134, 1323–1335.

Adams, D.S., Robinson, K.R., Fukumoto, T., Yuan, S., Albertson, R.C., Yelick, P., Kuo, L., McSweeney, M., Levin, M. (2006). Early, H+-V-ATPase-dependent proton flux is necessary for consistent left-right patterning of non-mammalian vertebrates. Development 133, 1657–1671.

Alenghat, F.J., Nauli, S.M., Kolb, R., Zhou, J., Ingber, D.E. (2004). Global cytoskeletal control of mechanotransduction in kidney epithelial cells. Exp Cell Res 301, 23–30.

Aragona, M., Panciera, T., Manfrin, A., Giulitti, S., Michielin, F., Elvassore, N., Dupont, S., Piccolo, S. (2013). A mechanical checkpoint controls multicellular growth through YAP/TAZ regulation by actin-processing factors. Cell 154, 1047–1059.

Bao, L., Locovei, S., Dahl, G. (2004). Pannexin membrane channels are mechanosensitive conduits for ATP. FEBS Lett 572, 65–68.

Batra, N., Burra, S., Siller-Jackson, A.J., Gu, S., Xia, X., Weber, G.F., DeSimone, D., Bonewald, L.F., Lafer, E.M., Sprague, E., *et al*. (2012). Mechanical stress-activated integrin α5β1 induces opening of connexin 43 hemichannels. Proc Natl Acad Sci USA 109, 3359–3364.

Beane, W.S., Morokuma, J., Adams, D.S., Levin, M. (2011). A chemical genetics approach reveals H,K-ATPase-mediated membrane voltage is required for planarian head regeneration. Chem Biol 18, 77–89.

Bernascone, I., Martin-Belmonte, F. (2013). Crossroads of Wnt and Hippo in epithelial tissues. Trends Cell Biol 23, 380–389.

Berridge, M.J., Lipp, P., Bootman, M.D. (2000). The versatility and universality of calcium signalling. Nat Rev Mol Cell Biol 1, 11–21.

Catterall, W.A. (2011). Voltage-gated calcium channels. Cold Spring Harb Perspect Biol 3, a003947–a003947.

Cherian, P.P., Siller-Jackson, A.J., Gu, S., Wang, X., Bonewald, L.F., Sprague, E., Jiang, J.X. (2005). Mechanical strain opens connexin 43 hemichannels in osteocytes: a novel mechanism for the release of prostaglandin. Mol Biol Cell 16, 3100–3106.

Chernet, B.T., Adams, D.S., Lobikin, M., Levin, M. (2016). Use of genetically encoded, light-gated ion translocators to control tumorigenesis. Oncotarget 7, 19575–19588.

Chernet, B.T., Fields, C., Levin, M. (2015). Long-range gap junctional signaling controls oncogene-mediated tumorigenesis in Xenopus laevis embryos. Front Physiol 5, 519–519.

Chernet, B.T., Levin, M. (2013). Transmembrane voltage potential is an essential cellular parameter for the detection and control of tumor development in a Xenopus model. Dis Model Mech 6, 595–607.

Coste, B., Mathur, J., Schmidt, M., Earley, T.J., Ranade, S., Petrus, M.J., Dubin, A.E., Patapoutian, A. (2010). Piezo1 and Piezo2 are essential components of distinct mechanically activated cation channels. Science 330, 55–60.

Dasari, V.R., Mazack, V., Feng, W., Nash, J., Carey, D.J., Gogoi, R. (2017). Verteporfin exhibits YAP-independent anti-proliferative and cytotoxic effects in endometrial cancer cells. Oncotarget 8, 28628–28640.

Dike, L.E., Chen, C.S., Mrksich, M., Tien, J., Whitesides, G.M., Ingber, D.E. (1999). Geometric control of switching between growth, apoptosis, and differentiation during angiogenesis using micropatterned substrates. In Vitro Cell Dev Biol Anim 35, 441–448.

Dupont, S., Morsut, L., Aragona, M., Enzo, E., Giulitti, S., Cordenonsi, M., Zanconato, F., Le Digabel, J., Forcato, M., Bicciato, S., *et al*. (2011). Role of YAP/TAZ in mechanotransduction. Nature 474, 179–183.

Ermakov, Y.A., Kamaraju, K., Sengupta, K., Sukharev, S. (2010). Gadolinium ions block mechanosensitive channels by altering the packing and lateral pressure of anionic lipids. Biophys J 98, 1018–1027.

Evans, W.H., De Vuyst, E., Leybaert, L. (2006). The gap junction cellular internet: connexin hemichannels enter the signalling limelight. Biochem J 397, 1–14.

Gjorevski, N., Nelson, C.M. (2010). Endogenous patterns of mechanical stress are required for branching morphogenesis. Integr Biol (Camb) 2, 424–434.

Gjorevski, N., Nelson, C.M. (2012). Mapping of mechanical strains and stresses around quiescent engineered three-dimensional epithelial tissues. Biophys J 103, 152–162.

Gomez, E.W., Chen, Q.K., Gjorevski, N., Nelson, C.M. (2010). Tissue geometry patterns epithelial-mesenchymal transition via intercellular mechanotransduction. J Cell Biochem 110, 44–51.

Halder, G., Johnson, R.L. (2011). Hippo signaling: growth control and beyond. Development 138, 9–22.

He, L., Tao, J., Maity, D., Si, F., Wu, Y., Wu, T., Prasath, V., Wirtz, D., Sun, S.X. (2018). Role of membrane-tension gated Ca(2+) flux in cell mechanosensation. J Cell Sci 131.

Holden, J.K., Cunningham, C.N. (2018). Targeting the Hippo pathway and cancer through the TEAD family of transcription factors. Cancers 10, 81.

Huberman, J.A. (1981). New views of the biochemistry of eucaryotic DNA replication revealed by aphidicolin, an unusual inhibitor of DNA polymerase alpha. Cell 23, 647–648.

Kang, S.G., Chung, H., Yoo, Y.D., Lee, J.G., Choi, Y.I., Yu, Y.S. (2001). Mechanism of growth inhibitory effect of Mitomycin-C on cultured

human retinal pigment epithelial cells: apoptosis and cell cycle arrest. Curr Eye Res 22, 174–181.
Kelkar, D.A., Chattopadhyay, A. (2007). The gramicidin ion channel: a model membrane protein. Biochim Biophys Acta (BBA)–Biomembranes 1768, 2011–2025.
Kim, J.H., Kushiro, K., Graham, N.A., Asthagiri, A.R. (2009). Tunable interplay between epidermal growth factor and cell-cell contact governs the spatial dynamics of epithelial growth. Proc Natl Acad Sci USA 106, 11149–11153.
Klapperstuck, T., Glanz, D., Hanitsch, S., Klapperstuck, M., Markwardt, F., Wohlrab, J. (2013). Calibration procedures for the quantitative determination of membrane potential in human cells using anionic dyes. Cytometry A 83, 612–626.
Kovács, M., Tóth, J., Hetényi, C., Málnási-Csizmadia, A., Sellers, J.R. (2004). Mechanism of blebbistatin inhibition of myosin II. J Biol Chem 279, 35557–35563.
Kuzma-Kuzniarska, M., Yapp, C., Hulley, P.A. (2016). Using fluorescence recovery after photobleaching to study gap junctional communication in vitro. Methods Mol Biol 1437, 171–179.
Kwon, M.S., Park, C.S., Choi, K., Ahnn, J., Kim, J.I., Eom, S.H., Kaufman, S.J., Song, W.K. (2000). Calreticulin couples calcium release and calcium influx in integrin-mediated calcium signaling. Mol Biol Cell 11, 1433–1443.
Lalande, M. (1990). A reversible arrest point in the late G1 phase of the mammalian cell cycle. Exp Cell Res 186, 332–339.
Levin, M. (2010). Bioelectric mechanisms in regeneration: unique aspects and future perspectives. Cell 20, 543–556.
Levin, M. (2014). Molecular bioelectricity: how endogenous voltage potentials control cell behavior and instruct pattern regulation in vivo. Mol Biol Cell 25, 3835–3850.
Levin, M., Sundelacruz, S., Levin, M., Kaplan, D.L. (2016). Role of membrane potential in the regulation of cell proliferation and differentiation. Stem Cell Rev 231–246.
Liu, Z., Wei, Y., Zhang, L., Yee, P.P., Johnson, M., Zhang, X., Gulley, M., Atkinson, J.M., Trebak, M., Wang, H.G., Li, W. (2019). Induction of store-operated calcium entry (SOCE) suppresses glioblastoma growth by inhibiting the Hippo pathway transcriptional coactivators YAP/TAZ. Oncogene 38, 120–139.
Lobikin, M., Chernet, B., Lobo, D., Levin, M. (2012). Resting potential, oncogene-induced tumorigenesis, and metastasis: the bioelectric basis of cancer in vivo. Phys Biol 9, 065002.
Lopez, W., Ramachandran, J., Alsamarah, A., Luo, Y., Harris, A.L., Contreras, J.E. (2016). Mechanism of gating by calcium in connexin hemichannels. Proc Natl Acad Sci USA 113, E7986–E7995.
Maric, D., Maric, I., Smith, S.V., Serafini, R., Hu, Q., Barker, J.L. (1998). Potentiometric study of resting potential, contributing K+ channels and the onset of Na+ channel excitability in embryonic rat cortical cells. Eur J Neurosci 10, 2532–2546.
Mathews, J., Levin, M. (2017). Gap junctional signaling in pattern regulation: Physiological network connectivity instructs growth and form. Dev Neurobiol 77, 643–673.
Nelson, C.M., Jean, R.P., Tan, J.L., Liu, W.F., Sniadecki, N.J., Spector, A.A., Chen, C.S. (2005). Emergent patterns of growth controlled by multicellular form and mechanics. Proc Natl Acad Sci USA 102, 11594–11599.
Ohata, H., Tanaka, K., Maeyama, N., Yamamoto, M., Momose, K. (2001). Visualization of elementary mechanosensitive Ca2+-influx events, Ca2+ spots, in bovine lens epithelial cells. J Physiol 532, 31–42.
Opsahl, H., Rivedal, E. (2000). Quantitative determination of gap junction intercellular communication by scrape loading and image analysis. Cell Adhes Commun 7, 367–375.
Ozawa, M., Engel, J., Kemler, R. (1990). Single amino acid substitutions in one Ca2+ binding site of uvomorulin abolish the adhesive function. Cell 63, 1033–1038.
Pai, V.P., Aw, S., Shomrat, T., Lemire, J.M., Levin, M. (2012). Transmembrane voltage potential controls embryonic eye patterning in Xenopus laevis. Development 139.
Pai, V.P., Martyniuk, C.J., Echeverri, K., Sundelacruz, S., Kaplan, D.L., Levin, M. (2016). Genome-wide analysis reveals conserved transcriptional responses downstream of resting potential change in Xenopus embryos, axolotl regeneration, and human mesenchymal cell differentiation. Regeneration 3, 3–25.
Pang, M.F., Siedlik, M.J., Han, S., Stallings-Mann, M., Radisky, D.C., Nelson, C.M. (2016). Tissue stiffness and hypoxia modulate the integrin-linked Kinase ILK to control breast cancer stem-like cells. Cancer Res 76, 5277–5287.
Patel, D., Zhang, X., Veenstra, R.D. (2014). Connexin hemichannel and pannexin channel electrophysiology: how do they differ? FEBS Lett 588, 1372–1378.
Pathak, M.M., Nourse, J.L., Tran, T., Hwe, J., Arulmoli, J., Trang, D., Le, T., Bernardis, E., Flanagan, L.A., Tombola, F., Cahalan, M.D. (2014). Stretch-activated ion channel Piezo1 directs lineage choice in human neural stem cells. Proc Natl Acad Sci USA 111, 16148–16153.
Piccolo, S., Cordenonsi, M., Dupont, S. (2013). Molecular pathways: YAP and TAZ take center stage in organ growth and tumorigenesis. Clin Cancer Res 19, 4925–4930.
Pietak, A., Levin, M. (2016). Exploring instructive physiological signaling with the bioelectric tissue simulation engine. Frontiers in Bioengineering and Biotechnology 4, 55–55.
Piotrowski-Daspit, A.S., Nerger, B.A., Wolf, A.E., Sundaresan, S., Nelson, C.M. (2017). Dynamics of tissue-induced alignment of fibrous extracellular matrix. Biophys J 113, 702–713.
Piotrowski-Daspit, A.S., Tien, J., Nelson, C.M. (2016). Interstitial fluid pressure regulates collective invasion in engineered human breast tumors via Snail, vimentin, and E-cadherin. Integr Biol (Camb) 8, 319–331.
Polio, S.R., Smith, M.L. (2014). Patterned hydrogels for simplified measurement of cell traction forces. Methods Cell Biol 121, 17–31.
Richardson, B.D., Saha, K., Krout, D., Cabrera, E., Felts, B., Henry, L.K., Swant, J., Zou, M.-F., Newman, A.H., Khoshbouei, H. (2016). Membrane potential shapes regulation of dopamine transporter trafficking at the plasma membrane. Nat Commun 7, 10423.
Sagar, G.D., Larson, D.M. (2006). Carbenoxolone inhibits junctional transfer and upregulates Connexin43 expression by a protein kinase A-dependent pathway. J Cell Biochem 98, 1543–1551.
Schlegelmilch, K., Mohseni, M., Kirak, O., Pruszak, J., Rodriguez, J.R., Zhou, D., Kreger, B.T., Vasioukhin, V., Avruch, J., Brummelkamp, T.R., Camargo, F.D. (2011). Yap1 acts downstream of alpha-catenin to control epidermal proliferation. Cell 144, 782–795.
Sjaastad, M.D., Lewis, R.S., Nelson, W.J. (1996). Mechanisms of integrin-mediated calcium signaling in MDCK cells: regulation of adhesion by IP3- and store-independent calcium influx. Mol Biol Cell 7, 1025–1041.
Tan, J.L., Liu, W., Nelson, C.M., Raghavan, S., Chen, C.S. (2004). Simple approach to micropattern cells on common culture substrates by tuning substrate wettability. Tissue Eng 10, 865–872.
Tseng, A., Levin, M. (2013). Cracking the bioelectric code: Probing endogenous ionic controls of pattern formation. Commun Integr Biol 6, e22595–e22595.
Verselis, V.K., Srinivas, M. (2013). Connexin channel modulators and their mechanisms of action. Neuropharmacology 75, 517–524.
Wallace, B. (1990). Gramicidin channels and pores. Annu Rev Biophys Biophys Chem 19, 127–157.
Wang, C., Zhu, X., Feng, W., Yu, Y., Jeong, K., Guo, W., Lu, Y., Mills, G.B. (2016). Verteporfin inhibits YAP function through up-regulating 14-3-3sigma sequestering YAP in the cytoplasm. Am J Cancer Res 6, 27–37.
Wu, J., Lewis, A.H., Grandl, J. (2016). Touch, tension, and transduction—the function and regulation of piezo ion channels. Trends Biochem Sci 42, 57–71.
Yang, M., Brackenbury, W.J. (2013). Membrane potential and cancer progression. Front Physiol 4, 185–185.
Zhou, Q.M., Wang, X.F., Liu, X.J., Zhang, H., Lu, Y.Y., Su, S.B. (2011). Curcumin enhanced antiproliferative effect of mitomycin C in human breast cancer MCF-7 cells in vitro and in vivo. Acta Pharmacol Sin 32, 1402–1410.